PROCEEDINGS B

royalsocietypublishing.org/journal/rspb

Research



Cite this article: Ciupe SM, Vaidya NK, Forde JE. 2021 Early events in hepatitis B infection: the role of inoculum dose. *Proc. R. Soc. B* **288**: 20202715.

https://doi.org/10.1098/rspb.2020.2715

Received: 29 October 2020 Accepted: 12 January 2021

Subject Category:

Ecology

Subject Areas:

immunology, theoretical biology

Keywords:

hepatitis B virus, mathematical models, inoculum dose

Author for correspondence:

Stanca M. Ciupe e-mail: stanca@vt.edu

Electronic supplementary material is available online at https://doi.org/10.6084/m9.figshare. c.5280331.

THE ROYAL SOCIETY

Early events in hepatitis B infection: the role of inoculum dose

Stanca M. Ciupe¹, Naveen K. Vaidya^{2,3,4} and Jonathan E. Forde⁵

SMC, 0000-0002-5386-6946; NKV, 0000-0003-3502-2464

The relationship between the inoculum dose and the ability of the pathogen to invade the host is poorly understood. Experimental studies in non-human primates infected with different inoculum doses of hepatitis B virus have shown a non-monotonic relationship between dose magnitude and infection outcome, with high and low doses leading to 100% liver infection and intermediate doses leading to less than 0.1% liver infection, corresponding to CD4 T-cell priming. Since hepatitis B clearance is CD8 T-cell mediated, the question of whether the inoculum dose influences CD8 T-cell dynamics arises. To help answer this question, we developed a mathematical model of virus-host interaction following hepatitis B virus infection. Our model explains the experimental data well, and predicts that the inoculum dose affects both the timing of the CD8 T-cell expansion and the quality of its response, especially the non-cytotoxic function. We find that a low-dose challenge leads to slow CD8 T-cell expansion, weak non-cytotoxic functions, and virus persistence; high- and medium-dose challenges lead to fast CD8 Tcell expansion, strong cytotoxic and non-cytotoxic function, and virus clearance; while a super-low-dose challenge leads to delayed CD8 T-cell expansion, strong cytotoxic and non-cytotoxic function, and virus clearance. These results are useful for designing immune cell-based interventions.

1. Introduction

The relationship between the inoculum dose (defined as the number of pathogens at the start of an infection) and the ability of the pathogen to invade and colonize the host is poorly understood. Uncovering this information will advance our knowledge of how the initial dose impacts immune responses and, consequently, long-term disease outcome. Host reactions against virus challenge are highly variable, ranging from immune tolerance, as in chronic infections with hepatitis B virus (HBV) [1], to adequate priming and disease control, as in mild infections with influenza and dengue viruses [2-4], to exacerbated responses leading to severe disease and death, as in respiratory infections with respiratory syncytial virus (RSV) and SARS-CoV-2 [5,6]. To determine whether variability in disease outcome is virus dependent, host dependent, inoculum dependent, or a combination of all these factors and more, one needs to investigate inoculum-outcome scenarios within the same animal model (or humans), infected with the same pathogen (or even the same pathogenic strain). In this study, we used data from chimpanzees infected with different doses of the same strain of hepatitis B virus to analyse the relationship between inoculum dose, host response, and disease outcome.

HBV is a DNA virus that infects liver cells (hepatocytes) of humans and results in either acute hepatitis or chronic disease [7], with the likelihood of progression to chronic illness being inversely correlated with the age of the patient [8]. Virus clearance is attributed to strong, diverse, and mature adaptive immune responses, with polyclonal and multispecific hepatic CD8 T-cell responses being the main factor in HBV removal [9–11]. Virus-specific CD8

¹Department of Mathematics, Virginia Tech, Blacksburg, 24060 VA, USA

²Department of Mathematics and Statistics, ³Computational Science Research Center, and ⁴Viral Information Institute, San Diego State University, San Diego, CA 92182, USA

⁵Department of Mathematics and Computer Science, Hobart and William Smith Colleges, Geneva, New York 14456, USA

T-cells contribute to both virus control and liver injury in hepatitis B virus infection [12,13]. Studies in chimpanzees and HBV-transgenic mice have shown that, in addition to causing viral hepatitis through production of cytotoxic granules that are able to directly kill the infected hepatocytes [14], HBV-specific CD8 T-cells inhibit virus replication inside a hepatocyte via non-cytotoxic processes mediated through production of interferon-γ (INF-γ) and tumour necrosis factor- α (TNF- α) [15–17]. The exact contribution of cytotoxic and non-cytotoxic processes to virus control is not clearly defined. Here, we are primarily interested in determining whether development of protective CD8 T-cell responses is dependent on inoculum dose. For this, we focused on published data from HBV-naive, immune-competent adult chimpanzees who were challenged with different doses of the same monoclonal HBV inoculum [18]. As revealed in the data, challenge with different inoculum doses resulted in different outcomes, including less than 0.1% liver infection, 100% liver infection without chronic infection, and 100% liver infection with persistent viremia. The outcomes were also related to CD4 T-cell kinetics, with early CD4 T-cell priming being associated with synchronized interhepatic CD8 T-cell response and viral clearance. Low virus challenge resulted in delayed CD4 T-cell, weak and poorly synchronized CD8 T-cell responses, and persistent viremia. The study suggested that the lack of virus control is due to compromised CD8 Tcell function, presumably due to lack of adequate priming and continuous expression of negative regulators that suppress antiviral functions and cause CD8 T-cell exhaustion [18]. While the role of CD8 T-cell in HBV clearance has been widely reported [9-11,19,20], the synergistic effects of CD8 and CD4 T-cells (such as CD4 T-cell help being needed for CD8 T-cell activation) deserve further quantification [21], as uncertainty remains on these issues, especially in the context of varying inoculum doses. Indeed, while the CD4 T-cell response was found to be strong and multispecific in acute HBV infections and relatively weak in chronic HBV patients [21], CD4 T-cell depletion at the peak of HBV infection did not show any effect on viral replication and liver disease [19]. Moreover, CD4 T-cell depletion in vaccinated chimpanzees who were re-challenged with HBV did not result in enhanced virus replication [22]. An important question is whether the relationship between the inoculum dose and the CD4 T-cell kinetics observed in the clinical study [18] translates into predictions for CD8 T-cell kinetics, such as expansion and function. Mathematical modelling can help answer these questions.

Mathematical models have provided a reliable platform for in-depth analysis, quantification, and mechanistic description of host-pathogen interactions [23-36]. In particular, they have been used to determine how inoculum dose correlates with pathogen kinetics and immune response development. Handel et al. [37] investigated the role of inoculum dose in virus kinetics during acute infections of pathogens such as adenovirus, infectious bronchitis, influenza A, and human parainfluenza viruses. They found that both innate and adaptive immune responses are needed to explain the inoculum dose-dependent data [38], and that protection and morbidity do not change monotonically with increased inoculum dose. Best et al. [25] showed that Zika virus infections with a lowdose challenge slow down virus dynamics (such as a longer time to the peak and clearance), but result in a similar viral burden as with the high-dose challenge. We previously investigated the role of the dose and characteristics of Simian Immunodeficiency Virus (SIV) inoculum in rhesus macaque infections and found that the structure of the inoculum (containing free virus, rather than virus-immune complexes) can explain higher infectivity of the virus during early infections [39]. In addition, several groups have used mathematical models to determine the role of the inoculum dose on CD8 T-cell expansion in the context of vaccination [40-42] and found that a medium dose leads to pathogenesis, high-dose leads to immune exhaustion, and a low dose leads to protection. Here, we develop a mathematical model of virus-host interaction following HBV infection and use it, together with data from HBV-infected chimpanzees, to determine the effect of the inoculum dose on CD8 T-cell development and function, resulting in various disease outcomes. In particular, we determine whether the incolulum doses affect the timing of CD8 T-cell expansion and/or the strength of cytotoxic or non-cytotoxic responses and, consequently, the dynamics of the virus, the extent of liver disease, and the infection outcomes.

2. Material and methods

(a) Model development

We model the interactions between six populations: uninfected hepatocytes, T; infected hepatocytes, I; hepatocytes refractory to reinfection, R; HBV virions, V; cytotoxic CD8 T-cells, E; and alanine transaminase (ALT), A (a chemical that measures the level of hepatic injury). We model proliferation of uninfected, infected, and refractory hepatocytes using logistic terms with the same per capita expansion rate r and carrying capacity T_m . In the presence of HBV, target cells become infected at rate β , and infected cells produce p new viruses per infected cell per day. Virus is cleared at rate c. Following HBV infection, naive HBV-specific CD8 T-cells, E, proliferate and either convert productively infected cells into refractory cells at rate ρ_r or produce cytotoxic granules that are able to directly kill infected cells at rate μ . The refractory class corresponds to either previously infected cells that are refractory to new infection because of the continuing effects of a non-cytotoxic immune response or infected cells that are not producing measurable amounts of virus [32]. However, because antigens may persist on the surface of refractory cells for some time [15], the refractory population may still be assayed as infected by antibody staining, and killed by cytotoxic CD8 T-cells. We assume CD8 T-cell-mediated killing of refractory cells occurs at the same rate μ . Since refractory cells have lost most or all of the replicative intermediates and covalently closed circular (ccc) DNA, they do not produce virus [15,43]. Both infected and refractory cells are killed by cytotoxic CD8 T-cells at rate μ , and infected hepatocytes are moved into the refractory class in the presence of cytokines produced by cytotoxic CD8 T-cells at rate ρ .

Following the successful resolution of the infection, CD8 T-cells contract and die, with a small number being replaced by memory cells. We model the CD8 T-cells expansion using a Hill-type function of time, with maximum population level e_0 , time of half-maximal expansion τ , and Hill coefficient n [44,45]. We assume that CD8 T-cells peak half a year post-infection and then contract to zero a year post-infection. We model the post-peak temporal pattern of contraction using a reverse of the Hill-type function used for expansion. Therefore, the CD8 T-cell population is given by

$$E(t) = \begin{cases} e_0 \frac{t^n}{\tau^n + t^n}, & t < 182.5, \\ e_0 \frac{(365 - t)^n}{\tau^n + (365 - t)^n}, & 182.5 \le t \le 365, \\ 0, & t > 365. \end{cases}$$
(2.1)

We also considered a more general model including the possible non-zero contraction phase (see electronic supplementary material). Our data fitting and model comparison showed that the model with non-zero contraction phase did not improve the fitting and the parameter estimates did not change from the estimates using the model (2.1). Therefore, we used model (2.1) for the dynamics during the study period and consider the extended model for sensitivity of the long-term dynamics.

Liver releases ALT at a constant rate s_A , corresponding to natural hepatocyte death, plus an immune-dependent rate proportional to the cytotoxic CD8 T-cell-induced infected and refractory hepatocyte killing ($\mu I E$ and $\mu R E$, respectively), with proportionality constant α . ALT is degraded at *per capita* rate d_A . The non-autonomous system of differential equations describing these interaction is given by

$$\frac{dT}{dt} = rT\left(1 - \frac{T + I + R}{T_m}\right) - \beta TV,$$

$$\frac{dI}{dt} = rI\left(1 - \frac{T + I + R}{T_m}\right) + \beta TV - \mu IE - \rho IE,$$

$$\frac{dV}{dt} = pI - cV,$$

$$\frac{dR}{dt} = rR\left(1 - \frac{T + I + R}{T_m}\right) + \rho IE - \mu RE,$$

$$\frac{dA}{dt} = s_A - d_A A + \alpha \mu IE + \alpha \mu RE.$$
(2.2)

Initial conditions are given by $T(0) = T_m$, I(0) = R(0) = 0, $V(0) = V_0$, and $A(0) = A_0 = s_A/d_A$, where V_0 is the normalized inoculum concentration and A_0 is the smallest ALT measurement for each subject.

3. Experimental data and parameter estimation

(a) Experimental data

For this study, we use HBV and ALT time series data from nine HBV-naive, adult chimpanzees previously published in Asabe *et al.* [18]. In addition, the data considered include the per cent of liver cell damage in these nine animals. HBV is measured in GE/ml, which we assume is a good proxy for infectious virus concentration [46]. We categorize the animals into two groups.

(i) CD4 T-cell-competent group

The first group consists of seven CD4 T-cell-competent subjects, who were inoculated with a serial dilution of the same monoclonal HBV inoculum. Briefly, one chimpanzee (subject A006) was infected with a high-dose inoculum of 10¹⁰ GE HBV DNA. This resulted in fast virus spread, 100% liver infection, elevated ALT (suggesting cytotoxic CD8 T-cell killing of infected cells), and eventual virus clearance by week 24. CD4 T-cell priming occurred three weeks after inoculation. Two chimpanzees (subjects A007 and 1622) were infected with a medium-dose inoculum of 10⁷ and 10⁴ GE HBV DNA, respectively. This resulted in low viral titres, less than 0.1% liver infection, elevated ALT (suggesting that cytotoxic CD8 T-cell killing is still happening), and faster virus elimination by weeks 9 and 7, respectively. CD4 T-cell priming occurred one and three weeks after inoculation, respectively. Two chimpanzees (subjects 1603 and 1616) were infected with a low-dose inoculum of 10 GE HBV DNA. This resulted in high virus titres, 100% liver infection, persistent viremia lasting for 42 and greater than 50 weeks (defined as chronic disease), respectively. CD4 T-cell priming occurred 13 weeks after inoculation in both subjects. Lastly, two chimpanzees (subjects 1618 and A014) were infected with a super-low-dose inoculum of 1 GE HBV DNA. This resulted in high virus titres, 100% liver infection, ALT elevation, and virus elimination by week 29 and 30, respectively. CD4 T-cell priming occurred seven weeks after inoculation in both subjects.

(ii) CD4 T-cell-control depletion subgroup

The second group consisted of two subjects (A2A007 and A3A005), challenged with a medium-dose inoculum of 10⁴ GE. Additionally, chimpanzee A2A007 was first immunodepleted of CD4 T-cells. This resulted in high virus titres, 100% liver infection, persistent viremia lasting for greater than 50 weeks, and no CD4 T-cell priming. By contrast, chimpanzee A3A005 was given an irrelevant control antibody. Surprisingly, unlike the previous medium-dose subjects, this resulted in high virus titres, 100% liver infection, ALT elevation, and virus elimination by week 26. CD4 T-cell priming occurred one week after inoculation.

The experimental results are summarized in electronic supplementary material, table S1.

(b) Parameter estimation

We fix several parameters to previously reported values. Since the weight of each animal is known (electronic supplementary material, table S1), we carry over the hepatocellularity numbers from human to chimpanzees as follows. It is known that the carrying capacity of the liver cells in a 70 kg human is 13.6×10^6 hepatocytes per ml [32]. Then, the carrying capacity of liver cells in a chimpanzee of weight w-kg can be calculated as $T_m = (13.6 \times 10^6/70) \times w$ hepatocytes per ml. We assume that all hepatocyte (uninfected, infected, and refractory) divide at per capita rate r = 1 per day [32,47]. Previous estimates for the virus clearance rate range from c = 0.69 per day [48–50], to c = 4.4 per day [51], to as high as c = 21.7 per day [52]. We chose c = 1.67 per day, corresponding to a viral half-life of 10 h. Based on preliminary fits, we observed the need for a high Hill-coefficient n for all subjects. We fix it to n = 15. The reported human values for plasma ALT half-life are $t_{1/2} = 47 \pm 10 \text{ h}$ [53]. We chose a half-life of 47 h, corresponding to ALT clearance rate $d_A = 0.35$ per day. We assume that ALT was at equilibrium before the start of the infection, and set the constant production rate to $s_A = A_0 d_A$.

Initial conditions are given by $T(0) = T_m$, I(0) = R(0) = 0, $V(0) = V_0$, and $A(0) = A_0$. V_0 is the inoculum dose normalized throughout 1.5 litres of blood (half of human amount for a 70 kg person, since the chimpanzees' weight varied between 16 and 50 kg): 6.6×10^6 GE per ml (for subject A006), 6.6×10^3 GE per ml (for subject A007), 6.6 GE per ml (for subjects 1622, A2A007, A3A005), 6.6×10^{-3} GE per ml (for subjects 1603 and 1616), and 6.6×10^{-4} GE per ml (for subject 1618 and A014). A_0 is chosen to be the smallest ALT measurement for each subject: 24 (for subject A006), 26 (for subject A007), 21 (for subject 1622), 27 (for subject 1603), 27 (for subject 1616), 30 (for subject 1618), 26 (for subject A014), 36 (for subject A2A007), and 42 (for subject A3A005). The parameters that are fixed across animals and initial values are summarized in electronic supplementary material, table S2.

The remaining parameters $\{\beta, \mu, \rho, p, \alpha, \tau\}$ are estimated by fitting models (2.2) and (2.1) to the experimental data.

Table 1. Best parameter estimates and fitting errors. SSQ, residual sum of squares.

subject	$\mu \times 10^{-4}$	$\beta \times 10^{-10}$	au (wk)	$\alpha \times 10^{-4}$	$ ho imes 10^{-4}$	р	SSQ
A006	4.1	0.37	6.7	1.2	4	7567	0.59
A007	2.4	0.62	6.4	207	6.7	2394	1.1
1622	4	1.8	8.4	191	6.7	452	0.71
1603	3.5	0.3	24.4	1.3	1.6	2142	0.53
1616	4.8	1.6	15	0.2	0.03	562	0.57
1618	2.8	0.2	14.8	0.9	3.4	6628	0.98
A014	4.1	0.22	15.6	4.1	2.4	1300	0.95
A2A007	2.8	0.39	16	0.9	0.3	4561	0.52
A3A005	4.4	0.25	13.6	2.6	2.9	1115	0.6
average	3.6	0.63	13.4	45	3.1	2969	
s.d.	0.8	0.61	5.6	87	2.4	2655	

(c) Fitting method

We use all HBV DNA ($V_{\rm data}$) and ALT ($A_{\rm data}$) data up to the first time when virus decays below the limit of detection ($V_{\rm data} < 10^2$ GE per ml) and do not consider any subsequent virus rebound. This corresponds to $N = \{19, 11, 13, 41, 47, 35, 39, 48, 26\}$ HBV data points and the same number of ALT data points for subjects A006, A007, 1622, 1603, 1616, 1618, A014, A2A007, and A3A005, respectively. In addition, data representing the empirical maximal percentage of liver infection ($L_{\rm tot}$), is $L_{\rm tot} = 100$ (for subjects A006, 1603, 1616, 1618, A014, A2A007, and A3A005) and $L_{\rm tot} = 0.1$ (for subjects A007 and 1622).

To estimate the remaining parameters, parm = { β , μ , τ , α , ρ , p}, we minimize the following functional:

$$J(\text{parm}) = \sum_{i=1}^{N} \left(\frac{\log_{10} V_{\text{data}}(t_i) - \log_{10} V(t_i)}{\max_i \log_{10} V(t_i)} \right)^2$$

$$+ \sum_{i=1}^{N} \left(\frac{\log_{10} A_{\text{data}}(t_i) - \log_{10} A(t_i)}{\max_i \log_{10} A(t_i)} \right)^2$$

$$+ \left(\frac{\max_i L(t) - L_{\text{tot}}}{\max_i L(t)} \right)^2,$$
(3.1)

where t_i and N are time points and the total number of time points, respectively, at which data were collected. Here, $V_{\rm data}(t_i)$ and $A_{\rm data}(t_i)$ are experimentally measured values of the HBV DNA and the ALT, respectively, at time t_i , while $V(t_i)$, and $A(t_i)$ are corresponding solutions given by model (2.2). Similarly, $\max_t L(t) = \max_t \ (100 \times I(t)/(T(t) + I(t) + R(t)))$ and $L_{\rm tot}$ represent the model prediction and the experimental measurement, respectively, for the maximum per cent of liver infection. We use a combined program with the 'fminsearch' optimizer and the 'ode45' solver in Matlab to simultaneously fit these three data sets (representative code in the electronic supplementary material).

4. Results

(a) Model versus data

The best estimate parameter values are given in table 1 and the solutions over time are shown in figures 1 and 2, along with the experimental data. Our model predictions agree with the

data well in each of the animals considered. This model is capable of describing the relation between inoculum dose and widely varying immune response and disease outcome.

(b) Virus dynamics

The viral dynamics predicted by our model indicates that high- (A006) and medium-dose (A007, 1622), immunecompetent chimpanzees showed rapid viral increase immediately post inoculation. The viral load in the high-dose, immune-competent chimpanzee (A006) reached a peak of 2×10^{10} GE/ml in three weeks post inoculation, where it plateaued for three weeks, and then decreased until it reached below the limit of detection at 15 weeks post inoculation (see figure 1, first panel). The medium-dose, immune-competent chimpanzees (A007 and 1622) showed low viral peaks of $3 \times$ 10⁷ and 10⁷ GE/ml, respectively, before decreasing to below the limit of detection at 10 and 12 weeks post inoculation, respectively (see figure 1, second and third panels). The low- and super-low-dose, immune-competent chimpanzees showed a three-week delay in viral increase. All of these subjects reach high viral peaks with values between 9×10^9 and 2×10^{10} GE/ml (see figure 1, fourth to seventh panels). One low-dose, immune-competent chimpanzee (1616) and the immune-depleted chimpanzee (A2A007) showed persistent viremia for 50 weeks and for the duration of the study (see figure 1, fifth and eighth panels). The other low-dose, immune-competent chimpanzee (1603) was viremic for 40 weeks post inoculation. For super-low-dose, immunecompetent chimpanzees (1618 and A014), viral load decays to below detection 35 and 36 weeks post inoculation. In these animals, the long-term simulation of model (2.2) with zero contraction of CD8 T-cell population (2.1) predicts viral rebound (see figure 1, sixth and seventh panels). Lastly and surprisingly, the medium-dose, immune-competent control chimpanzee (A3A005), showed a two-week delay in viral load increase, which reached a peak of 2×10^{10} GE/ml before decreasing below the limit of detection 25 weeks post inoculation (see figure 1, last panel).

We investigated virus-host parameters that may explain the differences in subjects' kinetics. We obtained similar inter-patient estimates for the infectivity rate, with average

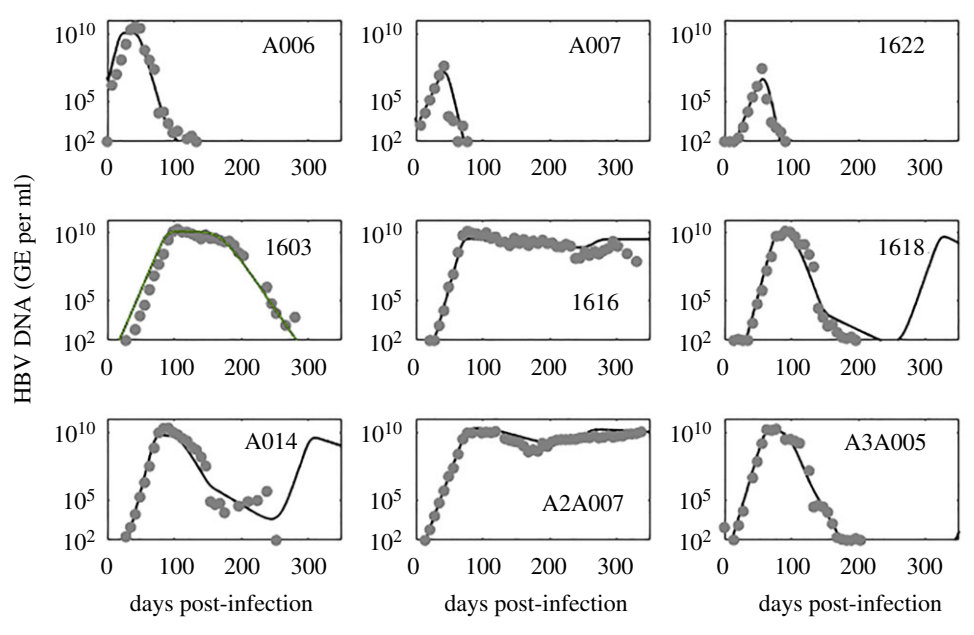


Figure 1. Virus dynamics over time as given by model (2.2) versus data. Parameters and initial conditions are given in electronic supplementary material, table S2; and table 1.

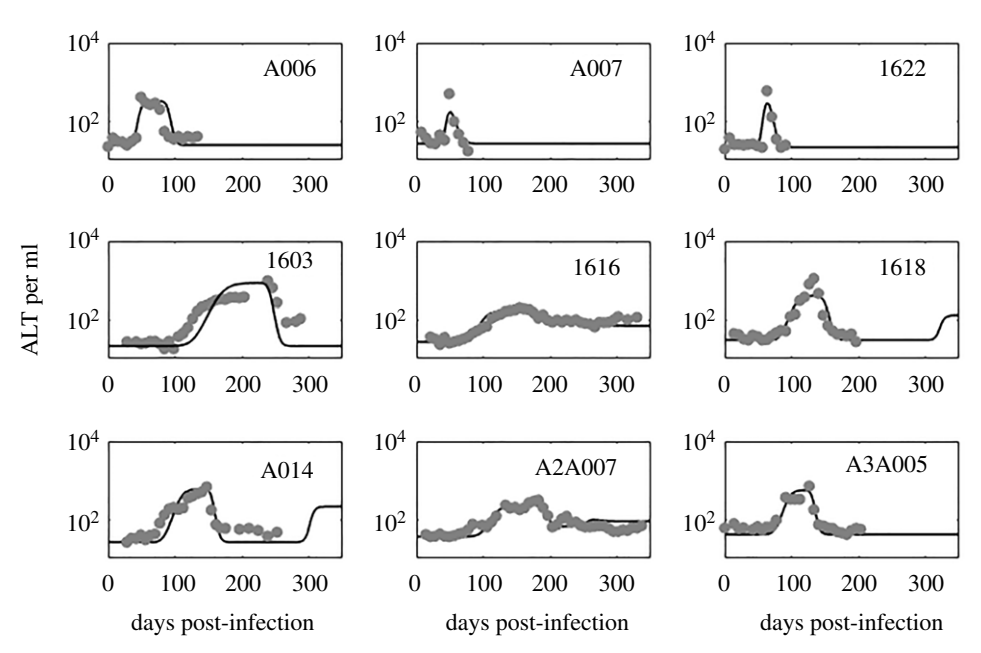


Figure 2. ALT dynamics over time as given by model (2.2) versus data. Parameters and initial conditions are given in electronic supplementary material, table S2; table 1.

 $\beta = 7.3 \times 10^{-11} \text{ ml/virus} \times \text{day}$ for group one 10^{-11} ml/virus × day when the second group is included), similar to the results from previous modelling work [32,47]. Since the magnitude of the clearance rate c is three orders of magnitude higher than that of the βT term in all patients, we could ignore the $-\beta TV$ virus loss term in the virus equation. The estimated virus production rate varied among subjects, with medium-dose, immune-competent subjects' average production rate (p = 1423 virus/infected cell×day) being half the high-, low-, and super-low-dose, subjects' average production rate ($p = 2969 \text{ virus/infected cell} \times$ day). Although we observed increased virus production in the seven subjects whose entire liver was infected, viral persistence did not always result from the highest virus production. For example, subject 1616, whose viremia persisted for the duration of the study, had the second lowest virus production rate and the highest infectivity rate.

We also estimated the viremia duration, defined by the time between challenge and the time post peak, when the virus reached below 10² GE/ml, and found good agreement with the empirical data used in data fitting (*values in electronic supplementary material, table S1). In these animals, viremia lasted 15 weeks for A006; 10.2 weeks for A007; 12 weeks for 1622; 40 weeks for 1603; greater than 50 weeks for 1616 and A2A007; 35 weeks for 1618; 36 weeks followed by rebound for A014; and 25 weeks for A3A005 (see electronic supplementary material, table S1 for comparison).

Using the per cent of infected cells over time predicted by model (2.2), $I/(T+I+R) \times 100\%$ (see electronic supplementary material, figure S1), we determined the time to reach maximal liver infection and the length of time spent at this level. We found that the entire liver is infected three weeks post challenge for the high-dose immune-competent subject. By contrast, the infection of the entire liver is delayed to 9.8

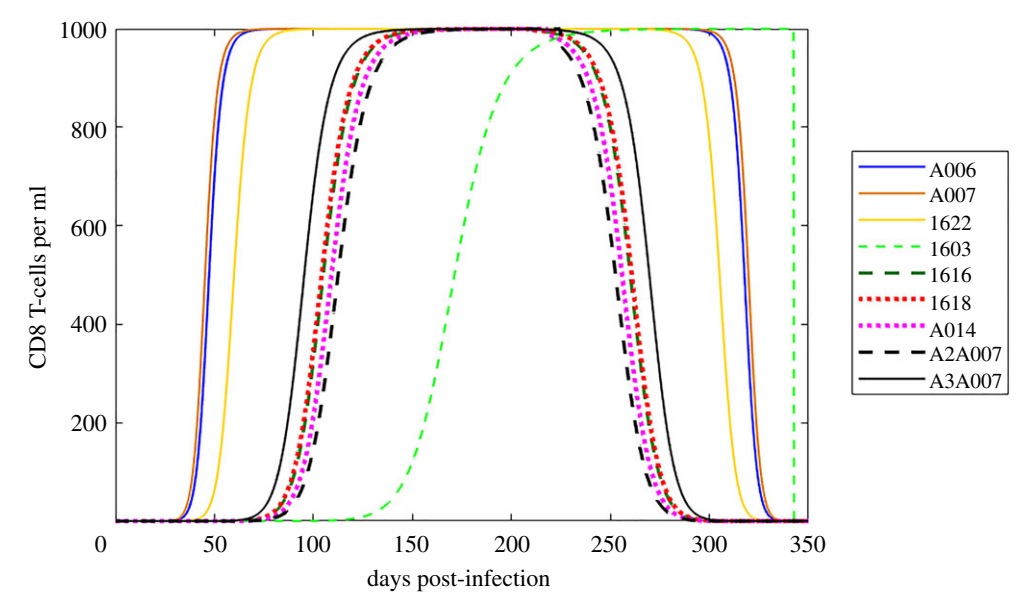


Figure 3. CD8 T-cell concentration, *E*, over time as given by model (2.1). Parameters and initial conditions are given in electronic supplementary material, table S2; table 1.

weeks post challenge for low- and super-low-dose immune-competent subjects and the immune compromised subject (with the exception of subject 1603, where peak liver infection occurred 11.7 weeks post challenge) and by 10 weeks in the medium-dose, immune-competent subject used as control. The maximum liver infection lasted for 6.7 weeks for the high-dose, immune-competent subject; 19 weeks and the duration of the study for the low-dose, immune-competent subjects; 7.8 and 9.8 weeks for the super-low-dose, immune-competent subjects; the duration of the study for the medium-dose, CD4 T-cell-depleted subject; and 9.1 weeks for the medium-dose, control subject. Our model predicted a maximum of 1.1% and 0.3% infection for the medium-dose, immune-competent subjects; occurring 6.4 and 7.9 weeks post challenge.

(c) Basic and effective reproductive numbers

We computed the basic and effective reproductive numbers over time, $R_0(t)$ and $R_{\rm eff}(t)$, which represent the average number of secondary hepatocyte infections resulting from a single infected cell in an entirely uninfected target cell population and a population composed of both uninfected and infected hepatocytes, respectively. They are given by

$$R_0(t) = \frac{\beta p T_m}{c(\mu + \rho) E(t)}, \quad R_{\text{eff}}(t) = \frac{T(t)}{T_m} \cdot R_0(t).$$
 (4.1)

As expected, the basic reproductive numbers are greater than 1 at the start of infection, consistent with the experimental data in which infection occurred in each animal. Assuming the level of the pre-infection CD8 T-cell responses as given by model (2.1), the basic reproductive numbers decay below 1 for five out of six animals with acute infections and one out of three with chronic disease (R_0 = 0.72 for A006, R_0 = 0.3 for A007 and 1622, R_0 = 0.74 for 1603, R_0 = 0.08 for A014, and R_0 = 0.06 for A3A005). By contrast, the basic reproductive numbers stay above 1 for the two animals with persistent viremia (R_0 = 1.01 for 1616 and R_0 = 1.18 for A2A007) and for one super-low-dose acute animal (R_0 = 1.03 for 1618) (see electronic supplementary material, figure S2, dashed lines). After the CD8 T-cell levels contract, the basic reproductive numbers increase above 1. Similarly, the effective reproductive numbers

decay below 1 for all animals due to combined high CD8 T-cell responses (high E) and low level of available uninfected target cells (small T/T_m), and rebound to values above 1 for all subjects following CD8 T-cell contraction (see electronic-supplementary material, figure S2, black solid lines).

(d) The relationship between inoculum dose, CD8 T-cell expansion, and CD8 T-cell function

The primary goal of this study is to determine whether there is a relationship between the times of CD4 T-cell priming observed experimentally and the CD8 T-cell dynamics given by population *E* in model (2.2). We will separate the results of the CD4 T-cell-depleted subject A2A007 from the rest of the subjects.

In the immune-competent subjects, the time of theoretical CD8 T-cell population's half-maximal expansion, τ , occurred 2 – 11.4 weeks later than the empirical CD4 T-cell priming, and did not follow the same patterns. Indeed, while one of the low-dose, immune-competent subjects (chimpanzee 1603) had the most delayed CD8 T-cell halfmaximal expansion time (24.4 weeks), the other low-dose, immune-competent subject (chimpanzee 1616) had a similar half-maximal expansion time to the super-low-dose subjects (at around 15 weeks post challenge). This contradicts the empirical CD4 T-cell priming, which occurred at the same time for both low-dose subjects (13 weeks post challenge) and much earlier for the super-low-dose subjects (seven weeks post challenge). The high-dose and medium-dose subjects had shorter half-maximal expansion times (6.7 weeks for A006; 6.4 and 8.4 weeks for A007 and 1622; and 13.6 weeks for A3A005). Indeed, while the theoretical CD8 T-cell population reached its maximum value of 10³ cells/ml early for the high- and medium-dose subjects, and late for one lowdose subject (1603), it has indistinguishable kinetics among the other low-dose and the super-low-dose subjects (figure 3). We found no difference in cytotoxic killing rates, μ , among the nine subjects, with average killing $\mu = 3.6 \times 10^{-4}$ per CD8 T-cell×day. However, while the non-cytotoxic rates $(\rho = 3.14 \pm 1.1 \times 10^{-4} \text{ per CD8 T-cell} \times \text{day})$ are similar among subjects with acute disease, they are reduced in subjects

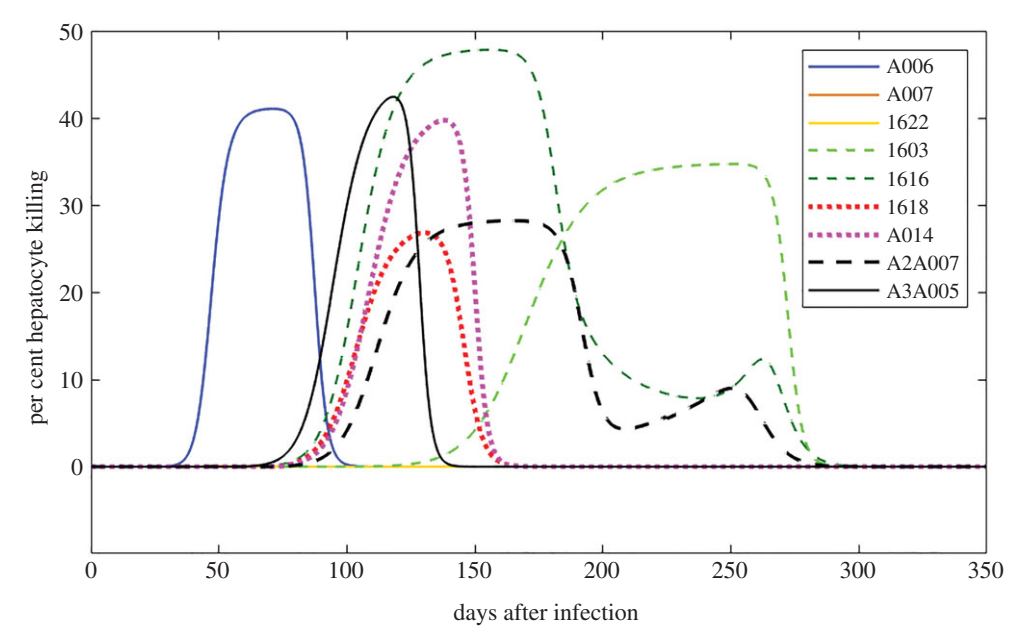


Figure 4. Percentage hepatocyte killing $(\mu l(t)E_8(t) + \mu E_8(t)R(t))/(T(t) + l(t) + R(t)) \times 100\%$ as given by model (2.2). Parameters and initial conditions are given in electronic supplementary material, table S2; table 1.

with chronic disease. For example, the low-dose chimpanzees 1603 and 1616 have non-cytotoxic rates $\rho=1.6\times 10^{-4}$ and $\rho=3\times 10^{-6}$ per CD8 T-cell×day, 2- and 100-times lower than the average. Moreover, the medium-dose CD4 T-cell-depleted chimpanzee A2A007 has a non-cytotoxic rate of $\rho=3\times 10^{-5}$ per CD8 T-cell×day, 10-times lower than the average. In addition, the CD4 T-cell-depleted chimpanzee has a lower cytotoxic killing rate $\mu=2.8\times 10^{-4}$ per CD8 T-cell×day (1.3-times lower than the average). This suggests that while CD4 T-cell depletion may not affect CD8 T-cell expansion, it affects the function of CD8 T-cells.

(e) The relationship between dose and overall pathology

We used our model to quantify the percentage of liver cells killed daily by the CD8 T-cells. From the model formulation, the percentage of liver cells killed by CD8 T-cells is given by

$$\kappa(t) = \mu E(t) \frac{I(t) + R(t)}{T(t) + I(t) + R(t)} \times 100\%.$$
(4.2)

Immune-mediated killing started four weeks after viral challenge for the high-dose subject (A006), and ceased 10 weeks later (see figure 4, blue solid curve). There is limited killing for two out of three immune-competent, medium-dose cases (A007 and 1622), with 0.1% and 0.085% peak liver loss, respectively (see figure 4, orange and yellow lines). The third immune-competent, medium-dose case (A3A005) had similar killing patterns as the high-dose case (see figure 4, black versus blue solid curves). This is associated with the small weight of the animal (14.6 kg, compared to the 35.4 kg for subject 1622), which allowed a higher inoculum dose per target cell causing faster virus spread. For low-dose subjects (1603 and 1616), immune-mediated killing started 18 and 11 weeks post inoculation, and persisted for a total of 20 and 18 weeks (see figure 4, dashed green curves). Similarly, the CD4 T-cell-depleted, medium-dose subject (A2A007) followed a killing pattern similar to the low-dose subjects: killing was delayed 12 weeks, was weak, and persisted for 25 weeks (see figure 4, dashed black curve). Lastly, for the super-low-dose,

immune-competent subjects (1618 and A014) the immune-mediated killing occurred 12 weeks post challenge and lasted for 10 weeks (see figure 4, dotted pink curves). Taken together, these results show that persistent infections, either induced by low inoculum doses or CD4 T-cell depletion, correlate with delayed and inefficient CD8 T-cell function and increased overall pathology.

(f) The relationship between CD8 T-cell expansion and ALT dynamics

ALT kinetics vary among subjects, with baseline ranging between 18 and 42 copies per ml. The expansion rates are similar among all subjects, except for A007 and 1622. These two subjects had limited liver cell infection (peak 1.1% and 0.3%, respectively), consistent with limited CD8 T-cellinduced loss. The ALT, however, was high for both subjects (see figure 2, second and third panel). To compensate for this, the ALT expansion rates were four-times higher than the average. Liver injury may have been induced by factors other than HBV infection (which have not been accounted for here). Interestingly, the CD4 T-cell-depleted subject (A2A007) had slight ALT elevation, suggesting liver injury. According to the model, this subject still has low CD8 T-cell cytotoxic activity, occurring in spite of the absence of CD4 T-cell help (see figure 2, eighth panel). Lastly, in some animals, the virus peak and subsequent decay did not always synchronize with ALT dynamics, with ALT staying elevated even after the virus was eliminated. This lack of linear correlation can be explained by our nonlinear model, which compensated for the difference in synchronization by allowing for cytotoxic-immune killing of the refractory cell population, which occurred (by design) at the same rate as the immune-induced killing of the infected population.

5. Discussion

In the current study, we developed a non-autonomous mathematical model of CD8 T-cell responses to hepatitis B

infection and used it, together with data from nine chimpanzees infected with a monoclonal HBV DNA, to determine the impact of different inoculum doses on CD8 T-cell development and function. One of the unique features in our model is the use of a non-autonomous term for the CD8 T-cell population given by a Hill-type function, in addition to inclusion of refractory cells. Having a common functional form in our model, with an identical but reverse pattern of expansion and contraction among subjects, allowed us to focus on differences among the subjects based on the time to half-maximal expansion, instead of being required to track individual CD8 T-cell populations.

The experimental study used here reported correlations between the inoculum dose, virus spread, and CD4 T-cell priming [18]. In particular, it found that high and super-lowdose inoculum (1010 GE and 1 GE) resulted in infection of the entire liver, which is cleared 15-36 weeks later, in the presence of CD4 T-cells. By contrast, a low-dose inoculum (10 GE) resulted in infection of the entire liver and virus persistence under delayed CD4 T-cell priming. A medium-dose inoculum $(10^4 \text{ and } 10^7 \text{ GE})$ resulted in limited infection (less than 0.1% of the liver), under fast CD4 T-cell priming. Lastly, a mediumdose inoculum under CD4 T-cell depletion resulted in virus persistence [18]. We used our novel model to investigate these undefined, complex relationships between empirically observed virus spread and CD4 T-cell priming, and to investigate the dynamics and function of the theoretically derived patterns of CD8 T-cell. We found no direct consistency between the timing of CD4 T-cell priming and the timing of CD8 T-cell expansion, defined here by the time of half-maximal expansion; the timing of CD8 T-cell half-maximal expansion is delayed up to 12.4 weeks compared to that of CD4 T-cell priming. We did, however, find an association between the overall outcome and the CD8 T-cell dynamics. In particular, CD8 T-cell populations expanded the fastest and viremia lasted for less than 15 weeks for subjects infected with a high- and medium-dose inoculum. For one subject infected with a low- and for subjects infected with a superlow-dose inoculum, medium expansion of CD8 T-cells occurred, and viremia lasted for 35-50 weeks. For the immune compromised subject infected with a medium-dose inoculum and for one immune-competent subjects infected with a low-dose inoculum, expansion of CD8 T-cells was the slowest and viremia persisted longer, past the end of the study.

We modelled both the cytotoxic and non-cytotoxic effects of CD8 T-cells, and found clear association between virus persistence and decreased non-cytotoxic function, independent of inoculum dose and CD4 T-cell status. In particular, both the immune-competent, low-dose subject (1616) and the immune compromised, medium-dose subject (A2A007), which were viremic throughout the study, had low CD8 T-cell non-cytotoxic functions: second-order and first-order magnitude lower than the average, respectively. By contrast, in the immune-competent chimpanzee infected with a lowdose inoculum, who had persistent viremia for 40 weeks before clearing the infection (1603), the CD8 T-cell noncytotoxic rate was reduced to half, compared with the average. We have previously noted the importance of noncytotoxic effects during acute adult human HBV infections, where the formation of cells refractory to reinfection was essential for preventing virus rebound [32,33]. In contrast to previous results, however, we report that cytotoxic effects against refractory cells are needed in order to explain prolonged ALT elevation even after virus (and consequently infected cells) are eliminated.

Studies in other virus infections, such as lymphocytic choriomeningitis virus (LCMV) [54,55], found the high-dose inoculum to be associated with immune exhaustion and virus persistence, while finding the low-dose inoculum to be associated with clearance. These studies correlated these outcomes to the priming of the adaptive immune responses by innate immune responses (mainly in the form of natural killer cells). It is known that hepatitis B is a stealth virus [56], hence innate immunity does not play a role in CD8 Tcell priming. The CD4 T-cells, on the other hand, might play this role. Indeed, if we look at the results from the perspective of CD8 T-cell immune responses, we find (as in previous studies [37,41,42]) that a fast and efficient CD8 Tcell response is associated with virus clearance, while a delayed and weak CD8 T-cell response is associated with virus persistence. Moreover, as seen in the chimpanzees with persistent viral infection (1616 and A2A007), the fact that immune responses are present, but inefficient in removing the virus, leads to increased pathology and liver scarring. The correlation between delayed CD4 T-cell priming and inefficient CD8 T-cell response (in particular non-cytotoxic effects), suggests that CD4 T-cell priming plays a role in the quality of the CD8 T-cell function.

Developing a suitable model that describes multiple data sets (viral load, ALT, liver infection) with a widely varying inoculum dose, leading to widely varying disease outcomes, was a challenging task. We considered several variants of model (2.2), including one without the refractory class and one with a constant CD8 T-cell population. Data fitting and model comparison analyses (not shown) allowed us to conclude that model (2.2), which includes both a refractory class and time varying (non-autonomous) CD8 T-cell population, best describes these data sets. Nevertheless, the model still has several limitations. We modelled CD8 T-cell responses using a non-autonomous function with the same maximal expansion level and contraction time for all nine subjects. It is possible that a different modelling approach may allow for inter-patient differences in CD8 T-cell population size, or a trade-off between CD8 T-cell population size and effectiveness. We found that, when CD8 T-cells contract to zero one year after infection, the HBV does not always decay below the limit of detection before rebounding (see super-low infected animal A014). If we assume, additionally, that the contraction results in non-zero CD8 T-cell levels, representative of the memory CD8 T-cell population, and/ or the contraction time is delayed (as observed in some of the subjects in [18]), virus decays below the limit of detection for all non-persistent cases (see electronic supplementary material, figure S3). In the chronic persistent cases (1616 and A2A007), however, changing the CD8 T-cell contraction level and/or the time of contraction, does not eliminate the virus. This is further confirmation that virus persistence is determined by weak CD8 T-cell non-cytotoxic function, rather than the duration of CD8 T-cell responses.

We chose a high Hill coefficient (n = 15), which suggests that the expansion from low to maximal CD8 T-cell values happens quickly. While n estimates favour lower values in some patients, it also favours higher values in others. To get further insight into this uncertainty, we performed semi-relative sensitivity analysis with respect to n. We found that V is sensitive to the changes in n during its

decay phase, with a peak positive influence occurring 12.7 weeks post-infection (see electronic supplementary material, figure S4, left). The Hill coefficient has a positive influence on the ALT curve as well, with a maximum effect at 6.7 weeks post-infection (the CD8 T-cell half-maximal stimulation rate). This is followed by no effect and a negative effect 12.7 weeks post-infection, at the peak positive effect on the virus (see electronic supplementary material, figure S4, right). The overall effects are weak, and do not influence early population profiles.

In summary, we developed a mathematical model of host-virus interactions in hepatitis B virus infection and used it to show that inoculum doses that result in delayed or absent CD4 T-cell responses are associated with delayed CD8 T-cell expansion and weak non-cytotoxic function and, consequently, result in virus persistence. Such results may inform the design of interventions.

Data accessibility. Data have been published before. Selected data and code were added to electronic supplementary material, S2.

Authors' contributions. Conceived and designed the study: S.M.C., J.E.F., N.K.V. Analysed the data: S.M.C. Wrote the paper: S.M.C., J.E.F.,

Competing interests. We declare we have no competing interests. Funding. The work of NKV was supported by National Science Foundation grant nos. DMS-1836647, DMS-1616299, and DMS-1951793, and by a UGP award from SDSU. SMC was supported by National Science Foundation grant no. 1813011.

References

- Bertoletti A, Ferrari C. 2012 Innate and adaptive immune responses in chronic hepatitis B virus infections: towards restoration of immune control of viral infection. Gut. 61, 1754–1764. (doi:10.1136/ qutjnl-2011-301073)
- 2. Smith AM, Perelson AS. 2011 Influenza A virus infection kinetics: quantitative data and models. WIREs: Syst. Biol. Med. 3, 429–445. (doi:10.1002/wsbm.129)
- Clapham HE, Tricou V, Van Vinh Chau N, Simmons CP, Ferguson NM. 2014 Within-host viral dynamics of dengue serotype 1 infection. J. R. Soc. Interface 11, 20140094. (doi:10.1098/rsif.2014.0094)
- Baccam P, Beauchemin C, Macken CA, Hayden FG, Perelson AS. 2006 Kinetics of influenza A virus infection in humans. *J. Virol.* 80, 7590–7599. (doi:10.1128/JVI.01623-05)
- Lee N et al. 2015 High viral load and respiratory failure in adults hospitalized for respiratory syncytial virus infections. J. Infect. Dis. 212, 1237–1240. (doi:10.1093/infdis/jiv248)
- Rockx B et al. 2020 Comparative pathogenesis of COVID-19, MERS, and SARS in a nonhuman primate model. Science 368, 1012–1015. (doi:10.1126/ science.abb7314)
- Fattovich G, Bortolotti F, Donato F. 2008 Natural history of chronic hepatitis B: special emphasis on disease progression and prognostic factors. *J. Hepatol.* 48, 335–352. (doi:10.1016/j.jhep.2007. 11.011)
- 8. Bennett JE, Dolin R, Blaser MJ eds. 2015 Mandell, Douglas, Bennett. Principles and Practice of Infectious Disease. Philadelphia: Elsevier Saunders.
- Isogawa M, Tanaka Y. 2015 Immunobiology of hepatitis B virus infection. *Hepatol. Res.* 45, 179–189. (doi:10.1111/hepr.12439)
- Publicover J et al. 2011 IL-21 is pivotal in determining age-dependent effectiveness of immune responses in a mouse model of human hepatitis B. J. Clin. Invest. 121, 1154–1162. (doi:10. 1172/JCI44198)
- Ferrari C. 1995 Hepatitis B virus immunopathogenesis. *Annu. Rev. Immunol.* 13, 29–60. (doi:10.1146/annurev.iy.13.040195.000333)

- Guidotti LG, Chisari FV. 1996 To kill or to cure: options in host defense against viral infection. *Curr. Opin. Immunol.* 8, 478–483. (doi:10.1016/S0952-7915(96)80034-3)
- Shin EC, Sung PS, Park SH. 2016 Immune responses and immunopathology in acute and chronic viral hepatitis. *Nat. Rev. Immunol.* 16, 509. (doi:10.1038/ nri.2016.69)
- Guidotti LG, Chisari FV. 2006 Immunobiology and pathogenesis of viral hepatitis. *Annu. Rev. Pathol. Mech. Dis.* 1, 23–61. (doi:10.1146/annurev.pathol.1. 110304.100230)
- Guidotti LG, Rochford R, Chung J, Shapiro M, Purcell R, Chisari FV. 1999 Viral clearance without destruction of infected cells during acute HBV infection. Science 284, 825–829. (doi:10.1126/ science.284.5415.825)
- Guidotti LG, Chisari FV. 2001 Noncytolytic control of viral infections by the innate and adaptive immuneresponse. *Annu. Rev. Immunol.* 19, 65–91. (doi:10.1146/annurev.immunol.19.1.65)
- Xia Y et al. 2016 Interferon-γ and tumor necrosis factor-α produced by T-cells reduce the HBV persistence form, cccDNA, without cytolysis.
 Gastroenterology 150, 194–205. (doi:10.1053/j. qastro.2015.09.026)
- Asabe S, Wieland SF, Chattopadhyay PK, Roederer M, Engle RE, Purcell RH, Chisari FV. 2009 The size of the viral inoculum contributes to the outcome of hepatitis B virus infection. J. Virol. 83, 9652–9662. (doi:10.1128/JVI.00867-09)
- Thimme R, Wieland S, Steiger C, Ghrayeb J, Reimann KA, Purcell RH, Chisari FV. 2003 CD8+ T cells mediate viral clearance and disease pathogenesis during acute hepatitis B virus infection. *J. Virol.* 77, 68–76. (doi:10.1128/JVI.77.1.68-76.2003)
- Isogawa M, Murata Y, Kawashima K, Tanaka Y. 2018 How are HBV-specific CD8+ T-cell responses induced? *Future Virol.* 13, 825–827. (doi:10.2217/ fvl-2018-0164)
- 21. Castellino F, Germain RN. 2006 Cooperation between CD4+ and CD8+ T cells: when, where, and how. *Annu. Rev. Immunol.* 24, 519–540. (doi:10.1146/annurev.immunol.23.021704.115825)

- Rybczynska J, Campbell K, Kamili S, Locarnini S, Krawczynski K, Walker CM. 2016 CD4⁺ T cells are not required for suppression of hepatitis B virus replication in the liver of vaccinated chimpanzees. J. Infect. Dis. 213, 49–56. (doi:10.1093/infdis/jiv348)
- Beauchemin CA, Handel A. 2011 A review of mathematical models of influenza A infections within a host or cell culture: lessons learned and challenges ahead. *BMC Public Health* 11, S7. (doi:10.1186/1471-2458-11-S1-S7)
- Ben-Shachar R, Koelle K. 2015 Minimal within-host dengue models highlight the specific roles of the immune response in primary and secondary dengue infections. J. R. Soc. Interface 12, 20140886. (doi:10. 1098/rsif.2014.0886)
- Best K, Perelson AS. 2018 Mathematical modeling of within-host Zika virus dynamics. *Immunol. Rev.* 285, 81–96. (doi:10.1111/imr.12687)
- Ciupe SM. 2018 Modeling the dynamics of hepatitis
 B infection, immunity, and drug therapy. *Immunol. Rev.* 285, 38–54. (doi:10.1111/imr.12686)
- Ciupe SM, Heffernan JM. 2017 In-host modeling. Infect. Dis. Model. 2, 188–202. (doi:10.1016/j.idm. 2017.04.002)
- 28. Nikin-Beers R, Ciupe SM. 2015 The role of antibody in enhancing dengue virus infection. *Math. Biosci.* **263**, 83–92. (doi:10.1016/j.mbs.2015.02.004)
- 29. Perelson AS. 2002 Modelling viral and immune system dynamics. *Nat. Rev. Immunol.* **2**, 28–36. (doi:10.1038/nri700)
- Neumann AU, Lam NP, Dahari H, Gretch DR, Wiley TE, Layden TJ, Perelson AS. 1998 Hepatitis C viral dynamics in vivo and the antiviral efficacy of interferon-α therapy. Science 282, 103–107. (doi:10.1126/science.282.5386.103)
- Banerjee S, Guedj J, Ribeiro RM, Moses M, Perelson AS. 2016 Estimating biologically relevant parameters under uncertainty for experimental within-host murine West Nile virus infection. J. R. Soc. Interface 13, 20160130. (doi:10.1098/rsif. 2016.0130)
- 32. Ciupe SM, Ribeiro RM, Nelson PW, Dusheiko G, Perelson AS. 2007 The role of cells refractory to productive infection in acute hepatitis B viral

- dynamics. *Proc. Natl Acad. Sci. USA* **104**, 5050–5055. (doi:10.1073/pnas.0603626104)
- Ciupe SM, Catllá AJ, Forde J, Schaeffer DG. 2011
 Dynamics of hepatitis B virus infection: what causes viral clearance? *Math. Popul. Stud.* 18, 87–105. (doi:10.1080/08898480.2011.564563)
- Carracedo Rodriguez A, Chung M, Ciupe SM. 2017 Understanding the complex patterns observed during hepatitis B virus therapy. Viruses 9, 117. (doi:10.3390/v9050117)
- Kadelka S, Ciupe SM. 2019 Mathematical investigation of HBeAg seroclearance.
 Math. Biosci. Eng. 16(6), 7616–7658. (doi:10.3934/ mbe.2019382)
- Forde JE, Ciupe SM, Cintron-Arias A, Lenhart S. 2016
 Optimal control of drug therapy in a hepatitis B model. *Appl. Sci.* 6, 219. (doi:10.3390/app6080219)
- Handel A, Li Y, McKay B, Pawelek KA, Zarnitsyna V, Antia R. 2018 Exploring the impact of inoculum dose on host immunity and morbidity to inform model-based vaccine design. *PLoS Comp. Biol.* 14, e1006505. (doi:10.1371/journal.pcbi.1006505)
- 38. Li Y, Handel A. 2014 Modeling inoculum dose dependent patterns of acute virus infections. *J. Theor. Biol.* **347**, 63–73. (doi:10.1016/j.jtbi.2014. 01 008)
- Ciupe SM, Miller CJ, Forde JE. 2018 A bistable switch in virus dynamics can explain the differences in disease outcome following SIV infections in rhesus macaques. Front. Microbiol. 9, 1216. (doi:10. 3389/fmicb.2018.01216)
- Rhodes SJ, Zelmer A, Knight GM, Prabowo SA, Stockdale L, Evans TG, Lindenstrøm T, White RG, Fletcher H. 2016 The TB vaccine H56⁺ IC31 doseresponse curve is peaked not saturating: data generation for new mathematical modelling

- methods to inform vaccine dose decisions. *Vaccine* **34**, 6285–6291. (doi:10.1016/j.vaccine.2016.10.060)
- Baral S, Antia R, Dixit NM. 2019 A dynamical motif comprising the interactions between antigens and CD8 T cells may underlie the outcomes of viral infections. *Proc. Natl Acad. Sci. USA* 116, 17 393–17 398. (doi:10.1073/pnas.1902178116)
- Johnson PL, Kochin BF, McAfee MS, Stromnes IM, Regoes RR, Ahmed R, Blattman JN, Antia R. 2011 Vaccination alters the balance between protective immunity, exhaustion, escape, and death in chronic infections. J. Virol. 85, 5565–5570. (doi:10.1128/JVI. 00166-11)
- Zhang YY, Zhang BH, Theele D, Litwin S, Toll E, Summers J. 2003 Single-cell analysis of covalently closed circular DNA copy numbers in a hepadnavirusinfected liver. *Proc. Natl Acad. Sci. USA* 100, 12 372–12 377. (doi:10.1073/pnas.2033898100)
- Mutua JM, Perelson AS, Kumar A, Vaidya NK. 2019 Modeling the effects of morphine-altered virus specific antibody responses on HIV/SIV dynamics. Sci. Rep. 9, 1–11. (doi:10.1038/s41598-019-41751-8)
- Mutua JM, Wang FB, Vaidya NK. 2020 Effects of periodic intake of drugs of abuse (morphine) on HIV dynamics: mathematical model and analysis. *Math. Biosci.* 326, 108395. (doi:10.1016/j.mbs.2020.108395)
- Gerlich WH. 2014 Reduction of infectivity in chronic hepatitis B virus carriers among healthcare providers and pregnant women by antiviral therapy. *Intervirology* 57, 202–211. (doi:10.1159/000360949)
- Ciupe SM, Ribeiro RM, Perelson AS. 2014 Antibody responses during hepatitis B viral infection. *PLoS Comp. Biol.* **10**, e1003730. (doi:10.1371/journal. pcbi.1003730)
- 48. Nowak MA, Bonhoeffer S, Hill AM, Boehme R, Thomas HC, McDade H. 1996 Viral dynamics in

- hepatitis B virus infection. *Proc. Natl Acad. Sci. USA* **93**, 4398–4402. (doi:10.1073/pnas.93.9.4398)
- Ishida Y et al. 2018 Acute hepatitis B virus infection in humanized chimeric mice has multiphasic viral kinetics. Hepatology 68, 473–484. (doi:10.1002/ hep.29891)
- Dahari H, Shudo E, Ribeiro RM, Perelson AS. 2009 Modeling complex decay profiles of hepatitis B virus during antiviral therapy. *Hepatology* 49, 32–38. (doi:10.1002/hep.22586)
- Murray J, Purcell R, Wieland S. 2006 The half-life of hepatitis B virions. *Hepatology* 44, 1117–1121. (doi:10.1002/hep.21364)
- Dandri M, Murray JM, Lutgehetmann M, Volz T, Lohse AW, Petersen J. 2008 Virion half-life in chronic hepatitis B infection is strongly correlated with levels of viremia. *Hepatology* 48, 1079–1086. (doi:10.1002/hep.22469)
- Kim WR, Flamm SL, Di Bisceglie AM, Bodenheimer HC. 2008 Serum activity of alanine aminotransferase (ALT) as an indicator of health and disease. Hepatology 47, 1363–1370. (doi:10.1002/hep.22109)
- Blattman JN, Antia R, Sourdive DJ, Wang X, Kaech SM, Murali-Krishna K, Altman JD, Ahmed R. 2002 Estimating the precursor frequency of naive antigen-specific CD8 T cells. J. Exp. Med. 195, 657–664. (doi:10.1084/jem.20001021)
- Moskophidis D, Lechner F, Pircher H, Zinkernagel RM. 1993 Virus persistence in acutely infected immunocompetent mice by exhaustion of antiviral cytotoxic effector T cells. *Nature* 362, 758–761. (doi:10.1038/362758a0)
- Wieland SF, Chisari FV. 2005 Stealth and cunning: hepatitis B and hepatitis C viruses.
 J. Virol. 79, 9369–9380. (doi:10.1128/JVI.79.15. 9369-9380.2005)